Journal of Alloys and Compounds 614 (2014) 63–70

Contents lists available at ScienceDirect

Journal of Alloys and Compounds

journal homepage: www.elsevier.com/locate/jalcom

Effects of minor Cu and Zn additions on the thermal, microstructure and tensile properties of Sn–Bi-based solder alloys

Jun Shen [a,*], Yayun Pu [a], Henggang Yin [a], Dengjun Luo [b], Jie Chen [a,c]

[a] College of Materials Science and Engineering, Chongqing University, Chongqing 400044, China
[b] Eunow Company Limited, Suzhou, China
[c] Chongqing Materials Research Institute Co., Ltd, Chongqing, China

ARTICLE INFO

Article history:
Received 28 March 2014
Received in revised form 3 June 2014
Accepted 3 June 2014
Available online 18 June 2014

Keywords:
Sn–Bi-based solder
Thermal property
Ultimate tensile strength
Elongation

ABSTRACT

The effects of Cu and Zn additions on microstructures, thermal and mechanical properties of Sn–Bi-based solder alloy were investigated. Thermal analysis indicated that Cu addition decreased both melting point and paste region of Sn–Bi-based solder while Zn played a reverse effect. Alloying Cu into binary solder resulted in an increase in both ultimate tensile strength and ductility. The improved strength of the Sn–40Bi–0.1Cu solder was attributed to the microstructural refinement and uniform distribution of the Cu_6Sn_5 intermetallic particles. The addition of Zn further depressed the precipitation of Bi, formed uniform globular $CuZn_2$ particles as well as flat blocky Cu_5Zn_8 phase. The enhanced strength of Zn-containing solder was ascribed to the presence of the globular $CuZn_2$ particles and structural refinement. Needle-like Zn with high aspect ratio forms at the position around the Bi-rich phase and leads a significant decrease of the elongation of Sn–40Bi–2Zn–0.1Cu solder. Fracture surface analysis indicated that the addition of Cu and Zn in Sn–Bi-based solder alloy did not affect the mode of fracture, and all tested solder exhibited brittle fracture with a pattern mixing with tongue and cleavage on the fracture surface.

1. Introduction

Solder joints provide the necessary electrical, thermal connection as well as mechanical support for different components and substrates in microelectronic devices [1–4]. Therefore, the performance and quality of the solders are crucial to the electronics assembly. Because of their relatively low-melting temperature, good solderability and high tensile strength [5–7], Sn–Bi lead-free solder alloys are widely used as an alternative of Sn–Pb solder. However, the bulky Bi-rich precipitates appeared in high Bi samples lead to a quick crack propagation, thus a wide range of additions such as Ni, Ga, RE element, graphene, and multi-wall carbon nanotubes are currently be alloyed with Sn–Bi solders [8–13] to improve the properties of solder joints. At present, many electronic devices are exposed to high temperature conditions that significantly decrease the fatigue life because of the excessive IMC layer. So, appropriate thickness of IMC layer is necessary to provide a proper bond and adhesion between the solder and metallization. Several beneficial effects of Zn or Cu addition to Pb-free solders have been reported [14,15]. Zn addition promoted the mechanical property of solder and also suppressed the growth of Cu_6Sn_5 IMC at the interface of solder and Cu substrate. Besides, Cu-containing solders have a lower corrosion resistance and higher mechanical strength. Taking these factors into considerations, Cu and Zn were adopted to synthesis the Sn–Bi-based alloys: Sn–40Bi–0.1Cu and Sn–40Bi–2Zn–0.1Cu. Moreover, thermal conductivity is the quantified ability of any materials to transfer heat and plays a critical role on the thermal performance of them [16,17]. Therefore, this work is devoted to investigate the effects of rare Cu and Zn additions on thermal properties, microstructures and mechanical properties of the newly developed Sn–Bi-based solder alloys.

2. Experimental procedures

In this study lead-free solder alloys of Sn–58Bi, Sn–40Bi–0.1Cu and Sn–40Bi–2Zn–0.1Cu were prepared by Sn, Bi, Zn and Cu (purity 99.99 wt.%) metal power. At first, the pre-weighted metal powders were well mixed with $CaCl_2$ flux to prevent oxidation in a graphite crucible. Then all these components were melted in medium frequency furnace at 280 °C. After that, molten solder in crucible was chill cast in steel molds to form two types of cylindrical ingots: one is with diameter of 30 mm and height of 230 mm, the other is with diameter of 60 mm and height of 60 mm.

* Corresponding author. Tel.: +86 23 13883111150.
E-mail address: shenjun@cqu.edu.cn (J. Shen).

http://dx.doi.org/10.1016/j.jallcom.2014.06.015
0925-8388/

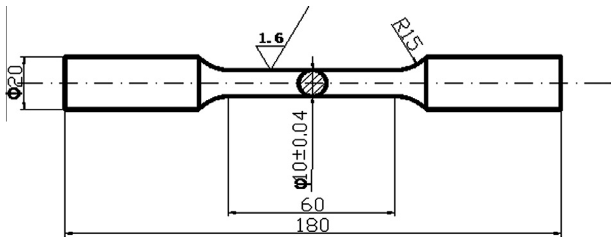

Fig. 1. Schematic illustration of the tensile test specimen.

2.1. Thermal properties

Five pieces of Sn–58Bi, Sn–40Bi–0.1Cu and Sn–40Bi–2Zn–0.1Cu solder specimens were machined from a cast ingot of 60 mm in diameter and 60 mm in height. Thermal conductivity of Sn–58Bi, Sn–40Bi–0.1Cu and Sn–40Bi–2Zn–0.1Cu solder alloys were measured with Transient Plane Source Method at 27 °C for 10 s, while the input power was 0.8 W.

Differential scanning calorimetry (DSC TGA/DSC 1/1100LF) was carried out to measure the melting process of three kind of solder alloys. The experiment procedure was that: 0.03 g prepared Sn–58Bi, Sn–40Bi–0.1Cu and Sn–40Bi–2Zn–0.1Cu solder balls were placed in an Al_2O_3 ceramic crucible and an empty crucible was taken as a reference. Then solder balls were heated from room temperature to 280 °C and then, maintained at this temperature for 5 min. After that, they were cooled down to room temperature at rate of 5 °C/min under Ar atmosphere protection.

2.2. Characterization

To observe the microstructures of three as-cast solder alloys, specimens were polished with diamond powders and etched with a solution of 5 vol.% HNO_3 + 92 vol.% C_2H_5OH + 3 vol.% HCl for a few seconds. The morphologies of as-cast specimens were examined by scanning electron microscope (SEM) (TESCAN, Inc. VegaII LMU) equipped with an energy dispersive X-ray spectroscopy (EDS) (OXFORD, Inc. ISIS300) analyzer.

2.3. Mechanical properties

The ultimate tensile strength and percentage of elongation of Sn–40Bi–2Zn–0.1Cu, Sn–40Bi–0.1Cu and Sn–58Bi solder alloys were evaluated by tensile tests. Fig. 1 shows the schematic illustration of specimens used in the tensile test. For each solder alloy (Sn–58Bi, Sn–40Bi–0.1Cu and Sn–40Bi–2Zn–0.1Cu), five specimens were machined from cast ingots of 30 mm in diameter and 230 mm in height. The specimens were annealed at 50 °C to remove the stress and strain induced by machining. For each solder alloy, tensile tests were conducted five times at the drawing speed of 1 mm/min at 25 °C. After the tensile tests, fracture surface of specimens were investigated through the scanning electron microscope (TESCAN VEGA 3 LMH SEM) as well as the energy dispersive X-ray spectroscopy (OXFORD, Inc. ISIS300 EDS).

3. Results and discussion

3.1. Thermal properties

Fig. 2 shows the DSC curves of Sn–58Bi, Sn–40Bi–0.1Cu and Sn–40Bi–2Zn–0.1Cu solder alloys upon heating at a scanning rate of 5 °C/min. The solidus temperatures, liquidus temperatures and mushy temperature zones of three solder alloys were collected in Table 1. With the addition of small amount of Cu element, the endothermic peak of Sn–58Bi solder decreased from 139 °C to 132.2 °C, whereas, an amount of 2% Zn added into Cu-containing solder led to an increase of the melting point of Sn–40Bi–2Zn–0.1Cu solder to 136.3 °C. This indicated that Cu element suppressed the melting point of Sn–Bi-based solder while Zn played a reverse effect. Moreover, Cu addition reduced the temperature interval of pasty range of Sn–58Bi solder from 27.2 °C to 22.0 °C, while the addition of Zn into Sn–40Bi–2Zn–0.1Cu expanded it slightly to 23.1 °C compared with Sn–40Bi–0.1Cu solder. It is well known that a promising solder alloy to form a reliable solder joint should have a low melting temperature and a narrow mushy temperature zone [18]. A narrower pasty range efficiently decreases the possibility of applied solder towards porosity and hot tearing. The heat of fusion (ΔH) of Sn–Bi-based solder alloys can be determined by Eq. (1) [19]:

$$\Delta H = \frac{KA}{m} \tag{1}$$

where K is constant by DSC system, which is defined as a calibration coefficient that depends on crucible shape and it can be regarded as a constant in the DSC system, m is the mass of the sample, and A is

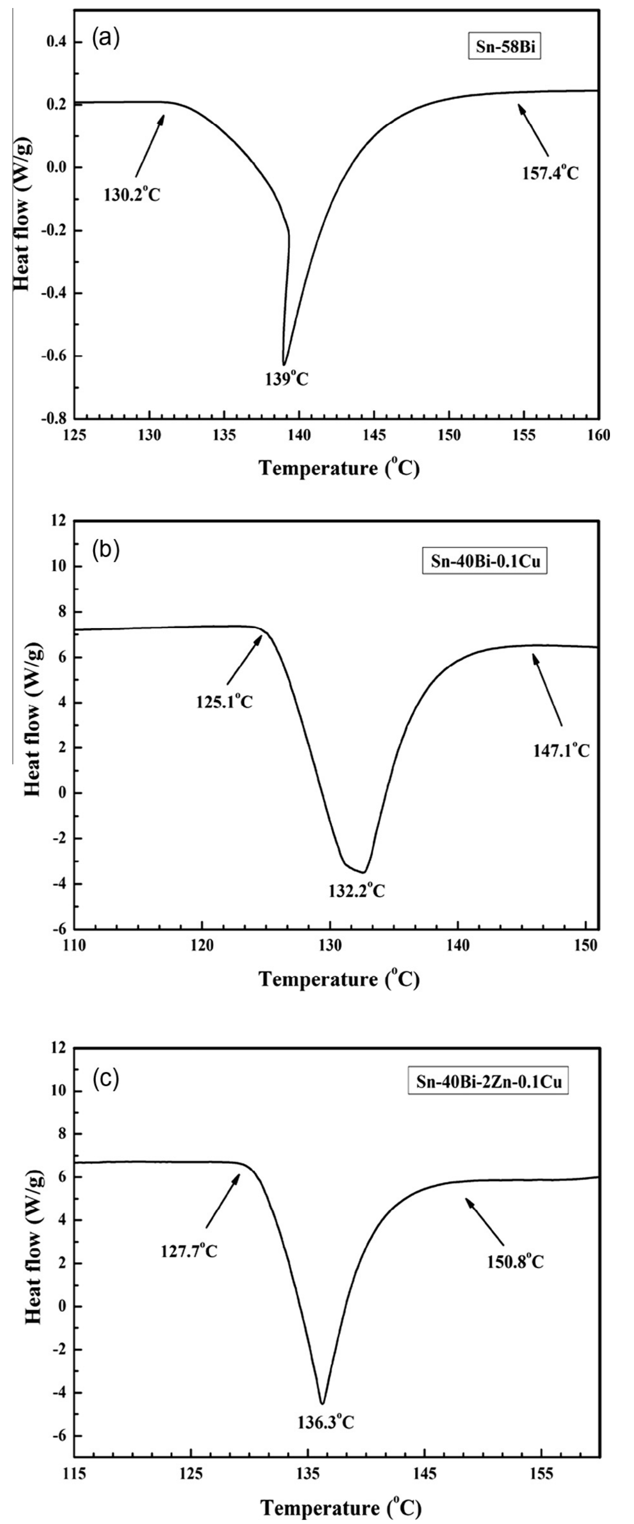

Fig. 2. DSC curves of the three solder alloys upon heating at a scanning rate of 5 K/min: (a) Sn–58Bi, (b) Sn–40B–0.1Cu, and (c) Sn–40Bi–2Zn–0.1Cu.

Table 1
The solidus temperatures, liquids temperatures, mushy temperature zones and mean thermal conductivity of the solder alloys.

Composition (wt.%)	Solidus temperature (°C)	Liquids temperature (°C)	Pasty range (°C)	Mean thermal conductivity (W/(mK))
Sn–58Bi	130.2	157.4	27.2	17.43 ± 0.6
Sn–40Bi–0.1Cu	125.1	147.1	22.0	20.48 ± 0.3
Sn–40Bi–2Zn–0.1Cu	127.7	150.8	23.1	24.51 ± 0.8

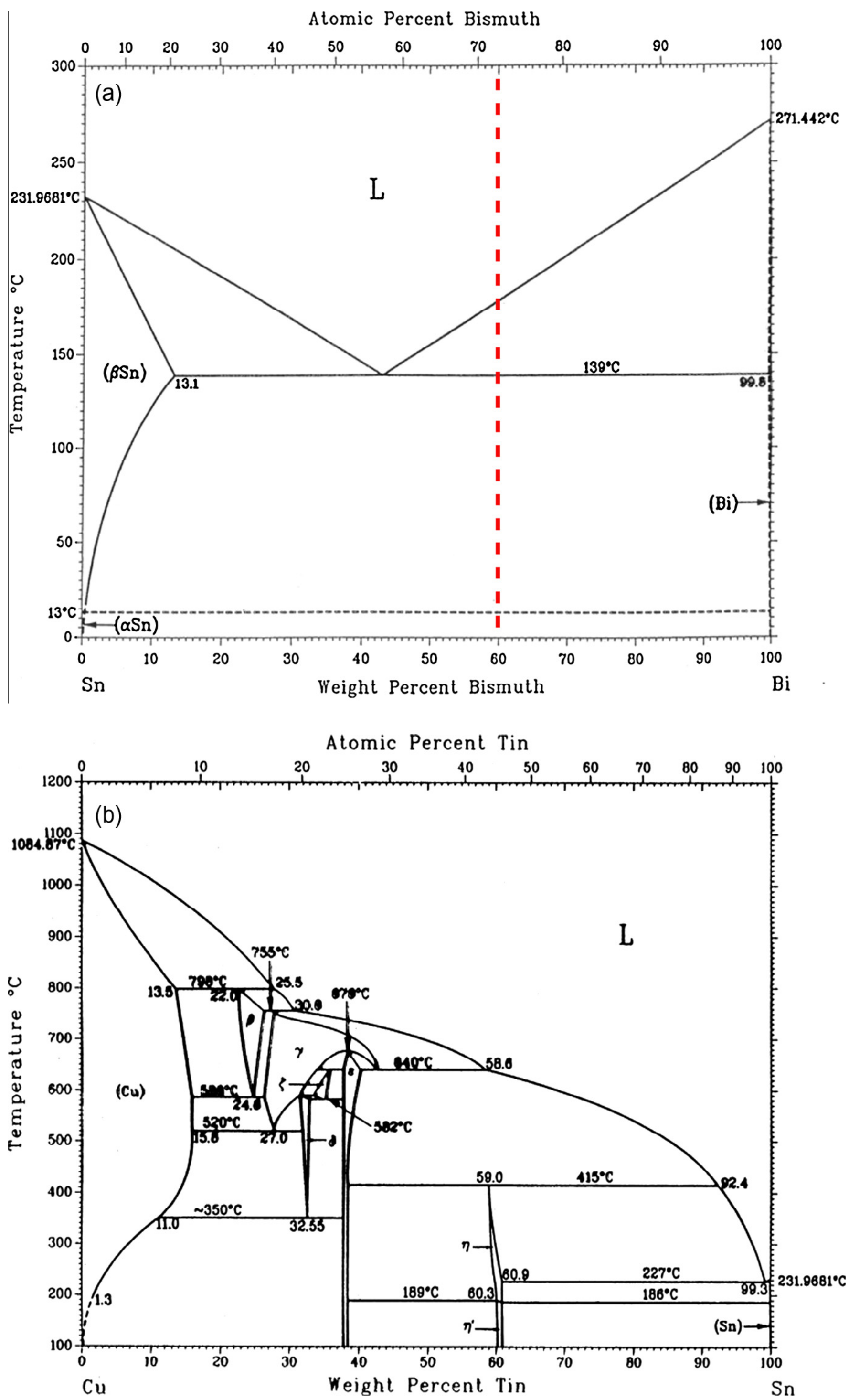

Fig. 3. The binary phase diagrams of (a) Sn–Bi [19] and (b) Sn–Cu [20].

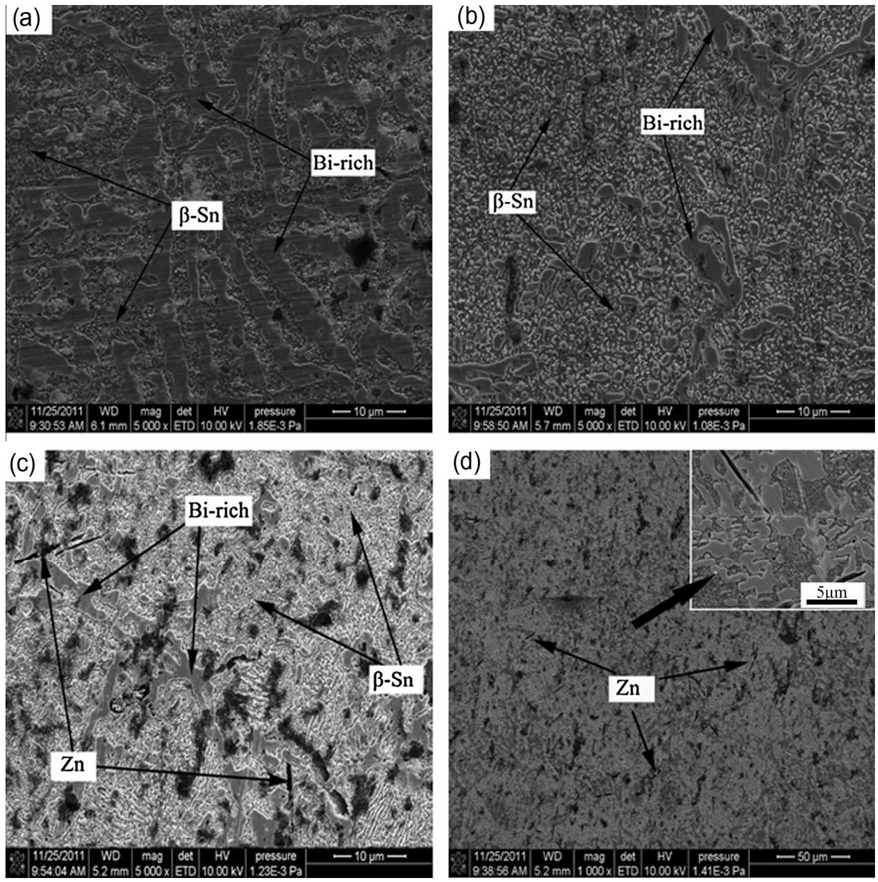

Fig. 4. SEM micrograph of: (a) Sn–58Bi, (b) Sn–40Bi–0.1Cu, (c) Sn–40Bi–2Zn–0.1Cu and (d) Zn-rich phase in Sn–40Bi–2Zn–0.1Cu.

the area below the endothermic peak. From Fig. 2 and DSC analysis software, the fusion heat of Sn–40Bi–0.1Cu solder was 47.00 J/g, while this value of Sn–40Bi–2Zn–0.1Cu solder dropped to 43.89 J/g, showing that the less energy was consumed for melting the Zn-containing solder.

Steady state method was carried out and Table 1 gives the mean value of thermal conductivity of three solder alloys. The thermal conductivity of Sn–40Bi–2Zn–0.1Cu solder (24.51 W/(mK)) was the highest of all and the Sn–40Bi–0.1Cu solder took the second place of 20.48 W/(mK), Zn and Cu additions obviously improved the thermal conductivity of Sn–Bi-based solder alloy. SEM (Fig. 4d) and XRD results (Fig. 6) show that Zn phase and Cu–Zn IMC uniformly distributed in the β-Sn phase of Sn–40Bi–2Zn–0.1Cu solder. Aksöz et al. [20] reported that the thermal conductivities of pure Zn is 120 W/(mK), which is higher than that of pure Bi (8 W/(mK)) and pure Sn (67 W/(mK)). This is the reason for the highest thermal conductivity of Sn–40Bi–2Zn–0.1Cu solder.

3.2. Microstructures

The microstructures of the as-cast Sn–58Bi, Sn–40Bi–0.1Cu and Sn–40Bi–2Zn–0.1Cu solder alloys are shown in Fig. 4. From Fig. 4a, dark rod-like Bi-rich phase with a great volume ratio dispersed in β-Sn matrix, which represented as bright regions and solidified primarily. Since the sample was a eutectic composition, bulky Bi-rich phase coarsened and its grain size was relatively large (20 um). To explain the microstructural evolution of Sn–Bi-based solder alloys, the equilibrium Sn–Bi phase diagram shown in Fig. 3a was used [21]. The solidification reaction of Sn–58Bi solder alloy from 280 °C to room temperature is: L (liquid) → L + eutectic (β-Sn + Bi-rich) → eutectic (β-Sn + Bi-rich) → eutectic (β-Sn + secondary precipitated Bi + Bi-rich). It suggested that Sn–58Bi solder was primarily composed of β-Sn matrix, a second precipitated Bi and Bi-rich phase.

The ability of alloying Cu to refine the grain size of Bi-rich phase was depicted in Fig. 4b. Compared with Sn–58Bi solder alloy, the number and size of Bi-rich phase in Sn–40Bi–0.1Cu solder significantly decreased. The morphology of Bi-rich phase shifted from a rod-like shape to spherical or irregular appearance, and the proportion of Bi-rich also reduced. The addition of Cu into Sn–40Bi–0.1Cu solder exhibited significant improvement in refinement of Bi-rich phase might be ascribed to two reasons. One is that Cu reacted with Sn to form Cu_6Sn_5 IMC particles, which themselves acted as heterogeneous nucleation sites and promoted a high nuclear intensity of Bi phase during solidification process. XRD and EDS analysis were also carried out to identify the type of the precipitated phase. According to Figs. 5a and 6a, Cu_6Sn_5 particles with a diameter about 4 μm were surrounded by Bi-rich phase and these two phases are coherent with each other very well. Even no obvious boundary was found in the adjacent region of them and their atoms seemingly had diffused into each other. EDS analysis confirmed that bits of Bi atoms actually existed in Cu_6Sn_5 phase. The explanation of this is given below. At the beginning of solidification (Fig. 3a and b [22]), Cu atoms reacted with Sn atoms to form Cu_6Sn_5 particles and separated out of liquid phase. As the temperature decreased, Bi atoms began to segregate and accumulate at the surface of Cu_6Sn_5 particles and gradually formed Bi-rich phase that wrapped the Cu_6Sn_5 compound. This can be supported by the similar crystallization orientation of Cu_6Sn_5 and Bi phase. It is also corresponding with the result that Bi atoms dissolved in the Cu_6Sn_5 phase during the reflow process reported by Zhang et al. [23]. The solidification reaction of Sn–40Bi–0.1Cu solder alloy from

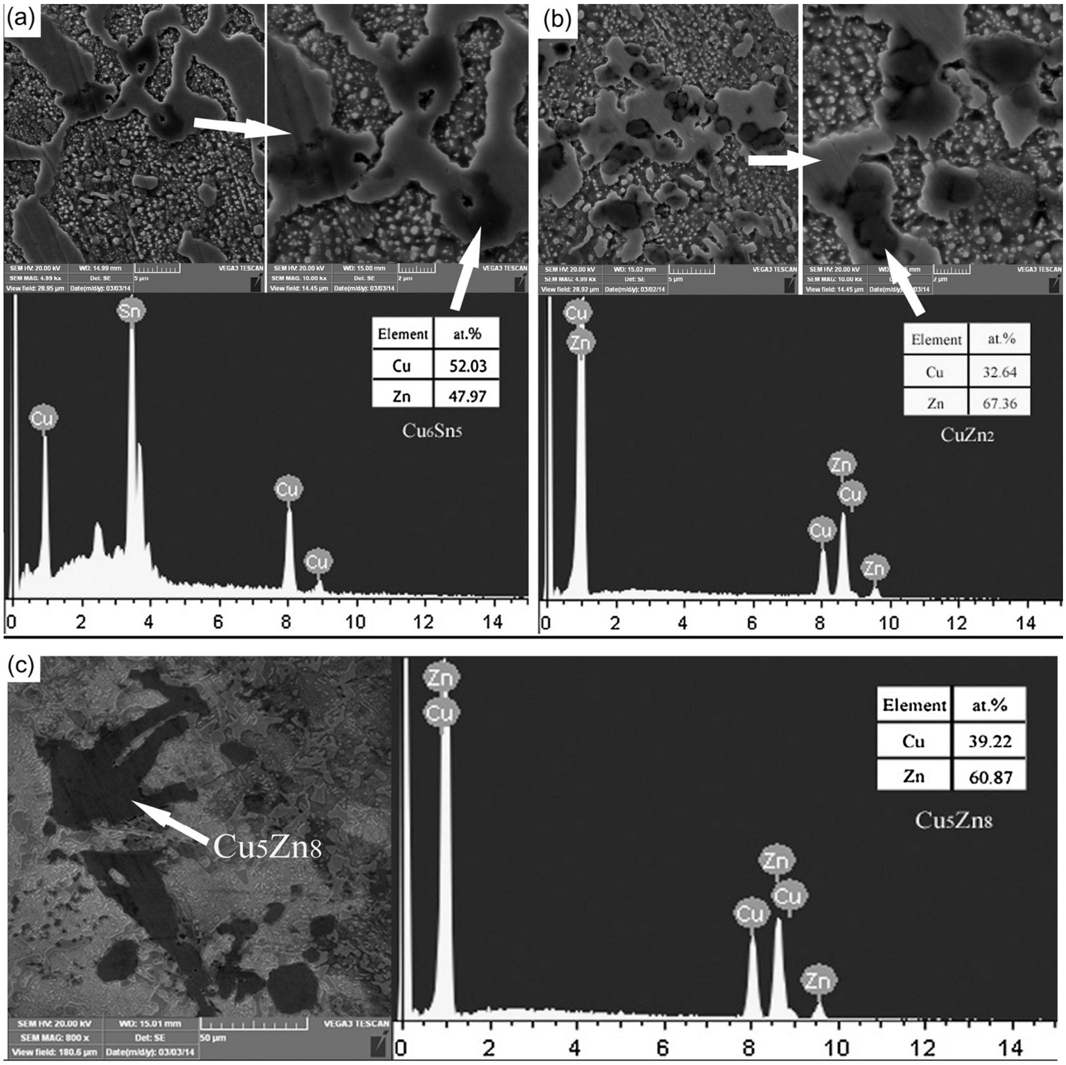

Fig. 5. SEM micrograph and correlative EDS analysis results of: (a) Cu_6Sn_5 phase in Sn–40Bi–0.1Cu, (b) $CuZn_2$ phase in Sn–40Bi–2Zn–0.1Cu, and (c) Cu_5Zn_8 phase in Sn–40Bi–2Zn–0.1Cu.

280 °C to room temperature (Fig. 3a) is L (liquid) → primary Sn + L → primary Sn + eutectic (β-Sn + Bi-rich) → primary Sn + secondary precipitated Bi + eutectic (β-Sn + secondary precipitated Bi + Bi-rich). This revealed that Bi particles precipitated twice and the rest of Gibbs free energy of original liquid solder had to devote themselves to remaining nucleation and evolution of other phases, which provided insufficient driving force for the growth of Bi phase. Thus, the depression of coarsening of Bi-rich phase was achieved after the addition of Cu element.

For Sn–40Bi–2Zn–0.1Cu solder alloy, Fig. 4c shows that the microstructure consisted of gray β-Sn phase, dendritic Bi-rich phase, secondary precipitated Bi and needle-like Zn-rich phase. The solidification reaction of Sn–40Bi–2Zn–0.1Cu solder alloy from 280 °C to room temperature is (Fig. 3a): L (liquid) → L + primary Sn → primary Sn + eutectic (β-Sn + Bi-rich) + eutectic (β-Sn + Zn-rich) → primary Sn + secondary precipitated Bi + eutectic (β-Sn + secondary precipitated Bi + Bi-rich) + eutectic (β-Sn + Zn-rich). Different with Sn–40Bi–0.1Cu solder alloy, Cu_6Sn_5 particles were not found in Sn–40Bi–2Zn–0.1Cu solder indicated that the formation of Cu–Zn IMC consumed all of Cu content because Cu has a higher affinity for reaction with Zn than Sn does. This is consistent with the researches reported by both Islam and Li [24,15]. According to XRD and EDS analysis (Figs. 5b and 6b), uniform globular $CuZn_2$ particles and blocky Cu_5Zn_8 were confirmed in Sn–40Bi–2Zn–0.1Cu solder. Zn atoms segregated from primary β-Sn matrix ahead of Bi and reacted with Cu atoms to form Cu–Zn IMC particles. Then, Bi atoms attached on the surface of Cu–Zn IMC particles to grow and ripen and gradually wrapped these primary-formed phases. Remnant Zn atoms gathered to form Zn-rich phase during solidification because Zn has a very low solubility within Sn [25]. These Zn-rich phases with shuttle-like shape were dissolved by etchant and mingled with Bi-rich phase (Fig. 4d).

Fig. 7 shows the microhardness of three solders as a function of alloy composition. As summarized in Table 2, the vickers hardness number of Sn–58Bi, Sn–40Bi–0.1Cu and Sn–40Bi–2Zn–0.1Cu solders are 18.58, 21.36 and 22.28, respectively. In general, the microhardness of a solder alloy is more sensitive to the microstructure of the solder, and higher hardness can be achieved since more alloying elements were added [26]. Fig. 4b and c represents the addition of Cu, Zn element into Sn–Bi-based solder alloy promoted precipitation hardening through forming IMC particles and transforming Bi-rich phase from bulky dendritic crystal into globular shape. Both the decrease in diameter of grain and the hinder of dislocation motion made contribution to a higher hardness value.

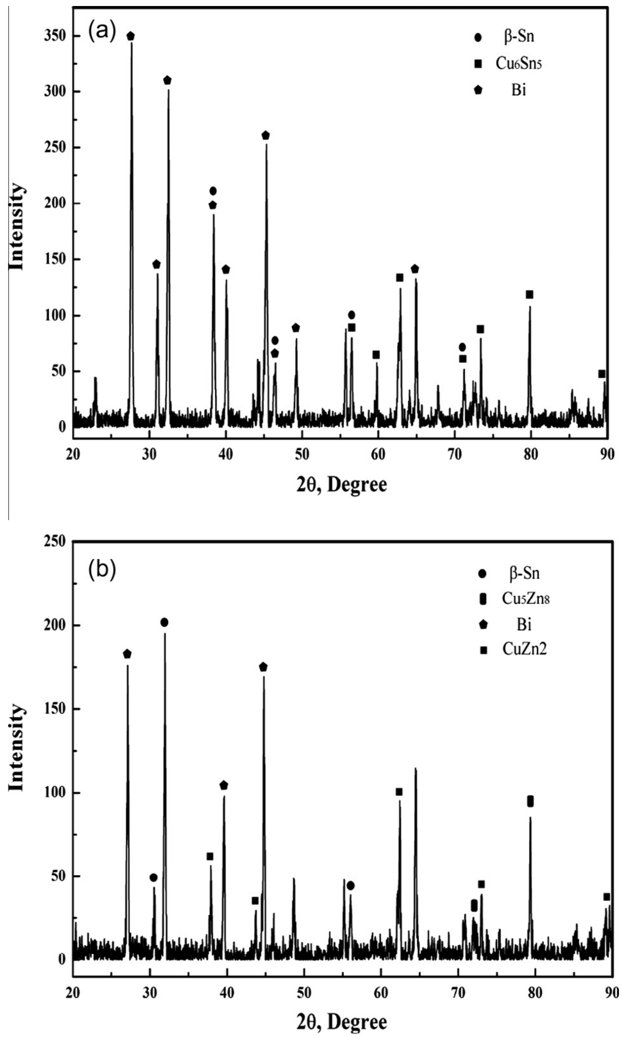

Fig. 6. XRD patterns of (a) Sn–40Bi–0.1Cu and (b) Sn–40Bi–2Zn–0.1Cu solder.

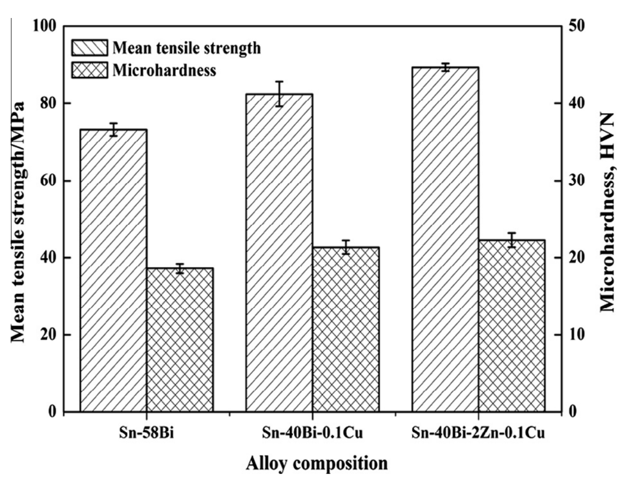

Fig. 7. The mean tensile strength and microhardness of Sn–58Bi, Sn–40Bi–0.1Cu and Sn–40Bi–2Zn–0.1Cu solder alloys.

3.3. Tensile property and fracture

Fig. 8 shows the stress–strain curves of Sn–58Bi, Sn–40Bi–0.1Cu and Sn–40Bi–2Zn–0.1Cu solder alloys with drawing speed of 1 mm/min at 298 K. Three solder alloys exhibited almost steady state flow after the stress levels climbed up to yield strength. The mean ultimate tensile strength (UTS) and elongation values are listed in Table 2. The Sn–40Bi–2Zn–0.1Cu solder had the highest UTS value of 89.31 MPa while Sn–58Bi reached the lowest value of 73.24 MPa. For Sn–40Bi–0.1Cu solder alloy, the value of UTS increased 12.6% to 82.45 MPa that compared with Sn–58Bi solder. According to aforementioned microstructural analysis for three solder alloys, the increment in UTS value of Sn–40Bi–0.1Cu solder was attributed to fine grained strengthening and precipitation strengthening mechanism. Smaller size of Bi phase dispersed in β-Sn matrix and resulted in higher strength of composite solder because of the increased number of dislocations. Moreover, refining globular shape Bi phase (diameter approximate 3 μm) enabled these particles to act as pins to prevent the motion of dislocation. Alloying Zn into composite solder formed amount of uniform spheroidal-shape $CuZn_2$ particles that enhanced the strength in similar way (Fig. 5b). Here $CuZn_2$ was regarded as secondary particle to capture the moving dislocation and for dislocations piling up [27,28]. Besides, this fine microstructure (Fig. 4d) with needle-shaped Zn uniformly distributed in Sn matrix was also effective in improving the strength of Sn–Bi-based solder alloys [29]. Overall, the Sn–40Bi–2Zn–0.1Cu solder achieved the best tensile property.

Table 2
Mean tensile strength and mean elongation of Sn–58Bi, Sn–40Bi–0.1Cu and Sn59.9Bi40Zn2Cu0.1 solder alloys.

Composition (wt.%)	Vickers hardness (Hv)	Mean tensile strength (MPa)	Mean elongation (%)
Sn–58Bi	18.58	73.24	24.8
Sn–40Bi–0.1Cu	21.36	82.45	35.4
Sn–40Bi–2Zn–0.1Cu	22.28	89.31	13.3

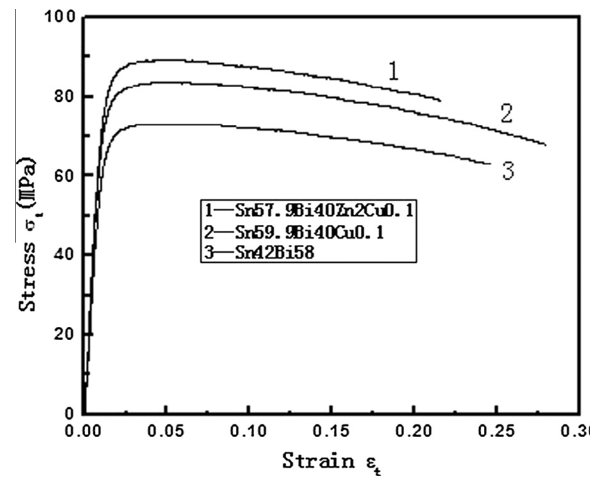

Fig. 8. The stress–strain curves of Sn–58Bi, Sn–40Bi–0.1Cu and Sn–40Bi–2Zn–0.1Cu alloys.

However, three solder alloys exhibited a different variation in elongation values. Sn–40Bi–0.1Cu solder had a value of 35.4% which was higher than Sn–58Bi solder (24.8%), and the lowest is Sn–40Bi–2Zn–0.1Cu solder with 13.3%. From Figs. 4d and 5, although Cu–Zn IMC particles occurred at the expense of Zn atom, there were quite amount of Zn-rich particles with a length about 20 μm dispersed in Sn–40Bi–2Zn–0.1Cu solder. Needle-like Zn particles with high aspect ratio constrained plastic flow during tensile deformation because the slip planes cannot move freely in their

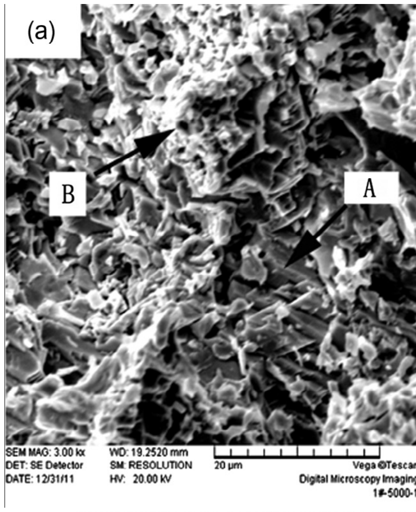

Point \ Element	Sn (at.%)	Bi (at.%)	Zn (at.%)
A	10.64	89.36	0.00
B	49.60	50.40	0.00
C	36.25	63.75	0.00
D	23.14	76.86	0.00
E	7.36	92.64	0.00
F	40.37	56.51	3.12

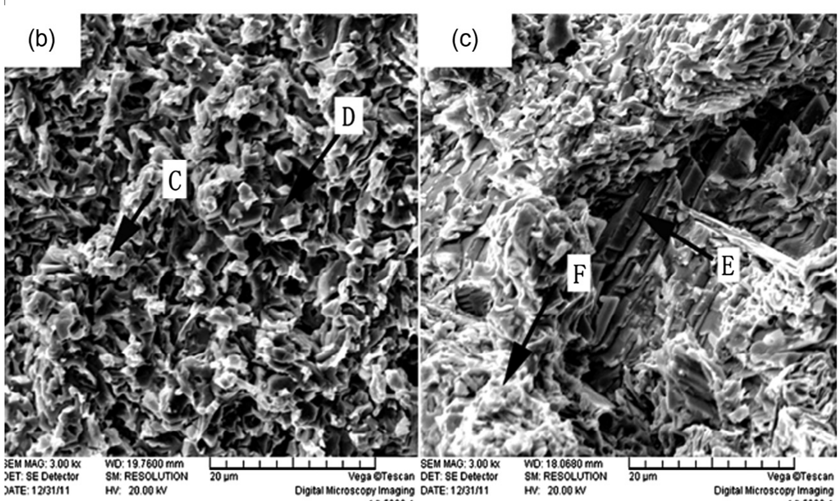

Fig. 9. The fracture surfaces and correlative EDS analysis results of (a) Sn–58Bi, (b) Sn–40Bi–0.1Cu and (c) Sn–40Bi–2Zn–0.1Cu alloys.

suitable direction which resulted in the lack of ductility. Furthermore, flat blocky Cu_5Zn_8 phase has a poor deformability which also prevented the motion of grain boundary. Therefore, elongation of Sn–40Bi–2Zn–0.1Cu solder was the worst of all, this result is similar with the previous study [30]. Compared with the Sn–58Bi and Sn–40Bi–2Zn–0.1Cu solder alloys, Sn–40Bi–0.1Cu solder alloy had a superior deformation resistance and long plastic region which make this solder alloy become one of the candidates for microelectronic packaging and interconnecting.

3.4. Fracture surfaces

Fig. 9 shows the fracture surfaces of Sn–58Bi, Sn–40Bi–0.1Cu and Sn–40Bi–2Zn–0.1Cu solder alloys after tensile tests. Sn–58Bi and Sn–40Bi–2Zn–0.1Cu solder displayed a mixed pattern with tongue and cleavage appearance in the fracture surface, which reflected a low ductility. From Fig. 9, the size of local cleavage region in Sn–40Bi–2Zn–0.1Cu solder alloy was the highest of all, which indicated that the ductility of Zn-containing solder alloy was the worst of these three solder alloys. While the microscopic fracture of Sn–40Bi–0.1Cu solder alloy was composed of tongues and exhibited the best ductility. According to the EDS result (Fig. 9), the cleavage planes was Bi-rich phase (point A and point F), the tongues (point B, point C, point D and point F) was Sn–Bi eutectic. The fracture of Sn–58Bi and Sn–40Bi–2Zn–0.1Cu solder alloys occurred in the brittle manner since the Bi-rich phase and Sn–Bi phase have limited ductility. In contrast to other two solder alloys, Sn–40Bi–2Zn–0.1Cu solder achieved the lowest elongation can be explained as below. Microstructural analysis of Sn–40Bi–2Zn–0.1Cu solder alloy has shown that needle-like Zn phase with poor elongation formed through Bi-rich phase. The formation of weak interface between Zn and Bi phase and the nature of poor deformability of Zn significantly deteriorated the ductility of Sn–40Bi–2Zn–0.1Cu solder and led to this fracture morphology. This is consistent with the elongation result in the tensile test of three solder alloys.

4. Conclusions

In this paper, three solder alloys of Sn–58Bi, Sn–40Bi–0.1Cu and Sn–40Bi–2Zn–0.1Cu were tested to evaluate the thermal property, microstructure and tensile property.

1. Cu addition decreased both melting point and paste region of Sn–Bi-based solder while Zn played a reverse influence.
2. The microstructures of the Bi-rich phase in both Sn–40Bi–0.1Cu and Sn–40Bi–2Zn–0.1Cu solder alloys were refined with the addition of Cu and Zn. A large portion of Bi phases converted into fine globular structures rather than rod-like lamella. A small number of Cu_6Sn_5 phase with odd-shape entrapped into

Bi-rich phase in Sn–40Bi–0.1Cu solder, which promoted the refinement of Bi dendrites. While for Sn–40Bi–2Zn–0.1Cu solder, uniform globular Cu_5Zn_8 particles and needle-like Zn-rich dispersed in Bi-rich phase and prompted the tensile strength of Bi-containing solder.

3. Both microhardness and tensile strength of Sn–Bi-based solder increased with the addition of Cu and Zn. The achieved strength improvement is caused by the refinement of microstructure and the formation of secondary particles in solder matrix. However, the ductility variation trend of three solder alloys is not consistent with that of tensile strength. Zn addition significantly decreased the elongation of Sn–40Bi–2Zn–0.1Cu solder owing to the formation of needle-like Zn-rich phase with high aspect ratio.

Acknowledgments

The projects are financially supported by a Natural Science Foundation of China (Grant No. 51375511) and Fundamental Research Funds for the Central Universities of China (Grant Nos. CDJZR12138801 and CDJZR13130033).

References

[1] J. Gorlich, D. Baither, G. Schmitz, Acta Mater. 58 (2011) 3187–3197.
[2] Q.Q. Li, Y.C. Chan, J. Alloys Comp. 567 (2013) 47–53.
[3] M.J. Esfandyarpour, R. Mahmudi, Mater. Sci. Eng., A 530 (2010) 402–410.
[4] J. Shen, M. Zhao, P. He, Y. Pu, J. Alloys Comp. 574 (2013) 451–458.
[5] Wislei R. Osório, Leandro C. Peixoto, Leonardo R. Garcia, J. Alloys Comp. 572 (2013) 97–106.
[6] T. Laurila, V. Vuorinen, Mater. Sci. Eng., R 68 (2010) 1–38.
[7] Yingxin Goh, A.S.M.A. Haseeb, Mohd Faizul Mohd Sabri, Electrochim. Acta 90 (2013) 265–273.
[8] G. Xu, F. Guo, X. Wang, J. Alloys Comp. 509 (2011) 878–884.
[9] S.K. Lin, T.L. Nguyen, S.C. Wu, Y.H. Wang, J. Alloys Comp. 586 (2014) 319–327.
[10] Wenxing Dong, Yaowu Shi, Zhidong Xia, J. Electron. Mater. 37 (2008) 982–991.
[11] Li Yang, Chengchao Du, Jun Dai, J. Mater. Sci.: Mater. Electron. 24 (2013) 4180–4185.
[12] X. Hu, Y.C. Chan, K. Zhang, K.C. Yung, J. Alloys Comp. 580 (2013) 162–171.
[13] Shenghong Zhang, Quanfang Chen, Compos. B Eng. 58 (2014) 275–278.
[14] S.K. Das, A. Sharif, Y.C. Chan, N.B. Wong, J. Alloys Comp. 481 (2009) 167–172.
[15] J.F. Li, S.H. Mannan, M.P. Clode, D.C. Whalley, Acta Mater. 54 (2006) 2907–2922.
[16] Esra Öztürk, Sezen Aksöz, Kazım Keşlioğlu, Necmettin Maraşlı, Thermochim. Acta 554 (2013) 63–70.
[17] K. Kiryukhina, H. Le Trong, Ph. Taihades, Scr. Mater. 68 (2013) 623–626.
[18] Janka Chriašteľová, Milan Ožvold, J. Alloys Comp. 457 (2008) 323–328.
[19] M.E. Brown, Introduction to Thermal Analysis, Chapman and Hall, New York, 1988. pp. 33.34.
[20] S. Aksöz, N. Maraşlı, K. Keşlioğlu, F. Yıldız, Thermochim. Acta 547 (2012) 1–5.
[21] I. Karakaya, W.T. Thompson, J. Phase Equilib. 14 (3) (1993) 525.
[22] S. Fürtauer, D. Li, D. Cupid, H. Flandorfer, Intermetallics 34 (2013) 142–147.
[23] Q.K. Zhang, H.F. Zou, Z.F. Zhang, J. Electron. Mater. 40 (2011) 2320–2328.
[24] M.N. Islam, Y.C. Chan, M.J. Rizvi, J. Alloys Comp. 400 (2005) 136–144.
[25] M. McCormack, S. Jin, J. Electron. Mater. 23 (1994) 715–720.
[26] D. Frear, H. Morgan, S. Burchett, J. Lau, The Mechanics of Solder Alloy Interconnects, Van Nostrand Reinhold, New York, 1994.
[27] Hu Xiaowu, Ke Li, Zhixian Min, J. Alloys Comp. 566 (2013) 239–245.
[28] G.E. Dieter, Mechanical Metallurgy, McGraw-Hill Book Co., New York, 1986.
[29] A.A. El-Daly, Y. Swilem, M.H. Makled, J. Alloys Comp. 484 (2009) 134–142.
[30] Jian Zhou, Yangshan Sun, Feng Xue, J. Alloys Comp. 397 (2005) 260–264.